LASER & PHOTONICS REVIEWS
www.lpr-journal.org

A New Thermodynamic Approach to Multimode Fiber Self-cleaning and Soliton Condensation

Mario Zitelli

A new thermodynamic theory for optical multimode systems is proposed. Theory is based on a weighted Bose–Einstein law, and includes the state equation, the fundamental equation for the entropy and a metric to measure the accuracy of the thermodynamic approach. The theory is used to compare the experimental results of two propagation regimes in multimode fibers, specifically the self-cleaning in the normal chromatic dispersion region and the soliton condensation in the anomalous dispersion region. Surprising similarities are found in terms of thermodynamic parameters, suggesting a common basis for the thermalization processes observed in the two propagation regimes.

1. Introduction

Multimode optical structures have been the subject of intense studies in the last decade. Multicore and multimode fibers, proposed half a century ago,[1,2] have been re-discovered to solve the problem of capacity crunch in optical transport networks,[3–5] or to generate high-quality power beams.[6] Photonic lattice have been proposed as flatbands for applications as slow light or novel photonic crystal fibers.[7] Multimode fibers were also proposed for high-resolution nonlinear fluorescence imaging.[8]

Under suitable conditions, multimodal systems can give rise to thermalisation processes, in which power distribution between system modes evolves irreversibly towards the thermodynamic equilibrium state of maximum Boltzmann entropy. In the weakly nonlinear regime, this process was initially described by the wave turbulence theory.[9,10]

In one of the first attempts to describe a complex optical system in thermodynamic terms,[11] the étendue of a light beam upon absorption and re-emission was compared to the thermodynamics of a two-dimensional gas. In ref. [12], the emission spectra of colloidal dye-doped laser was experimentally and theoretically analyzed, finding analogies with the Gross–Pitaevskii models for Bose–Einstein condensates. Experiments of beam self-cleaning in the normal dispersion region, an optical effect related to the inter-modal four-wave mixing (IM-FWM)[13,14] and taking place in multimode fibers, where the optical power flows towards the lower-order group of modes, were proposed in ref. [15], but only later[16,17] those effects were analyzed in thermodynamic terms and related to the thermalized states of a multimode fiber.

In ref. [18] a complete thermodynamic theory of optical multimode systems was introduced, using the Rayleigh-Jeans law (RJ) as the basic model for describing the power distribution among the system's modes; theory was developed for microcanonical ergodic systems with constant power P and internal energy U. The theory was applied to different multimode systems, such as a multimode graded-index fiber (GRIN), a nonlinear multicore Lieb waveguide lattice and a three-dimensional coupled cavity nonlinear system. An alternative derivation of the thermodynamic theory, still in terms of RJ law, was found in ref. [19]; by adopting a grand canonical description of the multimode system, maximization of the entropy was performed in terms of the probability density distribution of the system's microstates, obtaining a Gibbs distribution which was reduced to a RJ for the average mode power occupancy at thermal equilibrium.

The interplay of wave thermalization and linear disorder, represented by the linear random mode coupling (RMC) of multimode fibers,[20,21] was theoretically and experimentally analyzed in refs. [22] and [23]; a weak disorder was found to accelerate the rate of thermalization and condensation. In ref. [24] thermalized states were numerically calculated under a wide range of nonlinear conditions beyond the IM-FWM. These include second harmonic generation (SHG), multi-wave mixing (MWM) and optomechanical (OM) cascaded interactions between optical and mechanical modes. Steady states similar to thermalization were experimentally observed in ref. [25], in pseudo-linear systems composed by long spans of multimode GRIN fiber affected by RMC; output modal distribution were described in terms of a Bose–Einstein law.

Experimental self-cleaning thermalization was also observed in ref. [26], propagating 200-fs pulses at $\lambda = 1040$ nm wavelength, over few meters (0.5 to 1.5 m) of OM4 GRIN fiber supporting 110 modes per polarization. The GRIN fiber was chosen because its equally spaced propagation constants facilitate IM-FWM; coherent mode beating induces a periodic local intensity oscillation

M. Zitelli
Department of Information Engineering, Electronics and Telecommunications
Università degli Studi di Roma Sapienza
Via Eudossiana 18, 00184 Rome, Italy
E-mail: mario.zitelli@uniroma1.it

The ORCID identification number(s) for the author(s) of this article can be found under https://doi.org/10.1002/lpor.202400714

DOI: 10.1002/lpor.202400714

along the fiber, causing a longitudinal periodic modulation of the refractive index induced by the Kerr nonlinearity; in this context, IM-FWM is promoted by quasi-phase-matching conditions produced by the periodic index.[27] Output field was measured by off-axis digital holography and decomposed into a spectral resolved eigenmode basis.

A 3D modal decomposition method was applied in ref. [28] to analyze the condensation process during soliton propagation in 830 m of GRIN OM4 fiber. 250-fs pulses were propagated at $\lambda = 1400$ nm in the anomalous dispersion region of the fiber. Pulses at low power were separated by the modal dispersion, after having interacted by RMC and IM-FWM; for increasing power, a train of dispersive pulses converged to a train of quasi-solitons, and finally to a single soliton condensed to the fundamental mode.

Most of the listed works have relied on the RJ law to describe the distribution under thermalization conditions. The experimental methods used in refs. [26] and [28], however, have demonstrated particular accuracy in measuring the power distribution of the higher-order modes of a fiber (HOM), allowing a better analysis of the distributions.

In this work, we introduce a complete thermodynamic theory based on a weighted Bose–Einstein law (wBE); new expressions for the state equation and the fundamental equation of the Boltzmann entropy will be introduced; conditions for an increase of the entropy will be found; an optical Shannon or information entropy will be compared. The theory is assessed against the results of the last two experimental works, the former using one of the most accurate decomposition methods in a self-cleaning experiment in the normal dispersion regime, the latter propagating multimode solitons over long fiber spans. The wBE has proven higher accuracy respect to the RJ in reproducing the experimental modal distributions both in the thermalization regime induced by IM-FWM and in steady state regimes caused by the RMC; the accuracy is particularly evident in the description of the HOMS which, as it will be demonstrated, make a greater contribution to the entropy variation. Thermodynamic similarities are found between the self-cleaning regime of a GRIN fiber, in the normal chromatic dispersion region, and the multimode soliton condensation process in the anomalous dispersion region, similarities that allow a common thermodynamic description of two operationally different propagation regimes.

2. Theory

Commercial parabolic OM4 GRIN fibers are capable of propagating Q groups of Laguerre–Gauss degenerate modes; each group includes $g_j = 2j$ modes and polarizations, $j = 1, .., Q$. The total number of propagated modes and polarizations is $2M = Q(Q+1)$; the nearly degenerate modes of a group have substantially equal propagation constant[29] $\beta_j = n_{co}k_0\sqrt{1-2\Delta(j/Q)}$, with n_{co} the core index and $\Delta = (n_{co}^2 - n_{cl}^2)/2n_{co}^2$ the relative core-cladding index difference.

In this work, experiments are considered both in the normal and the anomalous chromatic dispersion regimes with variable input pulse peak power P (W). Correspondingly, it is scaled the power factor $\gamma = N/n_0 = P/P_0$, with N the total number of particles in the system, n_0 a reference number of particles (see Experimental Section), and P and P_0 the corresponding input peak powers.

In a generic multimode system, suppose that n_j is the bosonic population into modal group j, distributed over g_j nearly-degenerate modes and polarizations. $\epsilon_j = \beta_j - \beta_{j=Q}$ are the differential modal eigenvalues. In experiments where the input power and internal energy scale proportionally, the normalized internal energy $U_N = -\sum_j \beta_j n_j/N$ (1/m) and the normalized power $P_N = \sum_j n_j/N = 1$ are constant. Extremization of the optical entropy is solved by a weighted Bose–Einstein law (wBE, see the Experimental Section)[28]

$$|f_j|^2 = \frac{2(g_j-1)}{g_j\gamma}\frac{1}{\exp\left(-\frac{\mu'+\epsilon_j}{T}\right)-1} \tag{1}$$

In Equation (1), $|f_j|^2 = 2n_j/(\gamma n_0 g_j)$ is the mean modal power fraction, over two polarizations, in modal group j. $\mu' = \mu + \beta_{j=Q}$, with μ (1/m) the chemical potential and T (1/m) an optical temperature. μ' and T are two degrees of freedom for fitting Equation (1) to the experimental data, with the only constraint for the normalized power γ to scale with the input power, and to respect the conservation law $\sum_{j=1}^{Q} j|f_j|^2 = 1$.

Equation (1) has proven capable of reproducing the experimental modal power distributions in nonlinear thermalization regime, where IM-FWM dominates, and at lower power, where RMC is mostly responsible for power exchange among modes at least for long fiber spans.

The solution Equation (1) eventually applies to all experiments sharing the same normalized values U_N and P_N, for example those performed by increasing the input peak power while maintaining a same input distribution. Hence, it is meaningful to compare those experiments by fitting the modal distributions using Equation (1). In doing so, the validity of the thermodynamic approach is stressed using the error on the state equation (see Experimental Section)

$$\epsilon_{SE} = \frac{SE}{\sum_{j=1}^{Q}\beta_j\frac{g_j}{2}|f_j|^2 - \left(\mu' - \beta_{j=Q} + (2M-Q)\frac{T}{\gamma}\right)} \tag{2}$$

In Equation (2), μ' and T/γ must scale in order to balance the sum in the first part of the equation, which represents the normalized energy.

Equation (1) can be reduced to the well-known RJ law under the assumption $|\mu + \epsilon_j| << |Tn_0|$ (see Experimental Section). The RJ distribution has been widely used in the literature to analyze the modal power distribution in the thermalization regime.[18,23,26,30] In fact, it is an excellent criterion to recognize thermalized states. However, the assumptions made for its formulation prevent its use at lower power. The wBE is more effective to study modal distributions for variable input power, provided the error on the state equation (Equation 2) remains limited to below 5 %, which is a fair condition to certify the validity of the thermodynamic approach at a given power.

It has been previously reported[16] that, when approaching to the thermalization regime, the modal distribution approaches to the condensation into the fundamental mode $|f_1|^2$; the

temperature per unit power T/γ (T' in the RJ, see Experimental Section) reaches for a minimum value, the chemical potential $-\mu'$ approaches to the eigenvalue of the fundamental mode ϵ_1. The information or Shannon entropy S_S must decrease to a minimum as we approach to the condensation (see Experimental Section). These are typical signs of an achieved thermalization. In the following sections, it will be provided evidence of thermalization in self-cleaning experiments in the normal chromatic dispersion region, as well as in multimode soliton condensation experiments in the anomalous dispersion region. Results will be analyzed in terms of Boltzmann and Shannon entropy, temperature and chemical potential, after applying Equation (1) for fitting the experimental data.

3. Self-Cleaning Experiment

The first set of results come from the re-processing of previously reported experiments in the normal dispersion region.[26] Figure 2 of ref. [26] refers to a 0.5 m OM4 GRIN fiber, propagating 200-fs pulses at $\lambda = 1040$ nm wavelength. Figure 4 of the same paper refers to a 1.5 m OM4 GRIN fiber, with same input pulses; input peak power was varied from 2.5 to 86.7 kW. The output modal power fraction of $Q = 14$ modal groups was extracted by a combined method using both the output near-field (NF) and far-field (FF).

Figure S1 (Supporting Information) reports the power fraction of the modes versus ϵ_j (red dots), in the experiment of Figure 2b in ref. [26] at 52 kW input peak power. Statistical power fluctuations are observed for the modal power into each group, which should not be considered as experimental errors; by averaging the modal power fractions into the groups we obtain $|f_j|^2$ (black circles) which are not affected by statistical fluctuations and can be fitted using the RJ (Equation 7) or the wBE (Equation 1); fits are calculated using a standard nonlinear least squares method. In the thermalization regime, the former law can reproduce the experimental data up to the 8-th modal group (36 modes per polarization), while the latter is accurate up to the 14-th group (105 modes per polarization). From the RJ, we obtain $T' = 400$ (1/m), $\mu' = -72626$ (1/m) and the fit R-square = 0.958; from the wBE it is $T = 25283$ (1/m), $\mu' = -72388$ (1/m), $T/\gamma = 361$ (1/m) and the R-square = 0.996. The error on the state equation ϵ_{SE} is 0.008 for the wBE and 0.002 for the RJ.

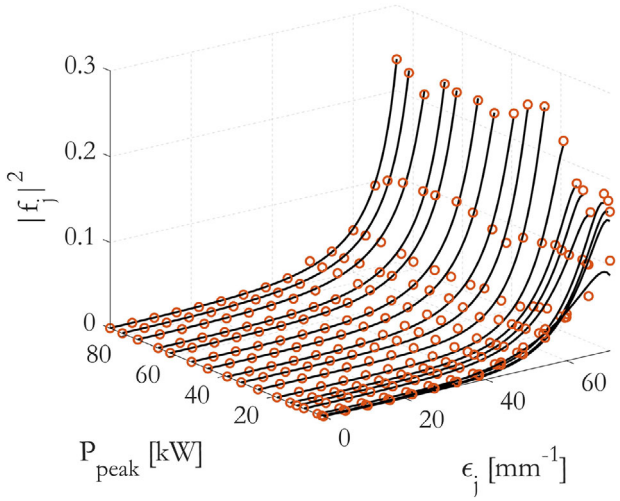

Figure 1. Output mean modal power fraction $|f_j|^2$ versus modal group eigenvalues and input peak power. 200-fs pulses were propagated over 1.5 m of GRIN at $\lambda = 1040$ nm. Post-processing from experimental data in Figure 4 of ref. [26]

By proceeding in a similar way with the experiment of Figure 4 in ref. [26], we obtain the wBE and RJ fits illustrated in Figure S2 (Supporting Information). Here, it is more evident the larger accuracy obtained using the wBE when reproducing the mean modal power fraction of the HOMs. In **Figure 1**, they have resumed the mean modal power fractions $|f_j|^2$ versus ϵ_j and the input peak power P from Figure 4 in ref. [26]. Black curves are the fits performed using Equation (1). **Table 1**

Table 1. Thermodynamic parameters for the experiment of Figure 1.

	RJ				wBE					Entropy			
P [kW]	T' [m^{-1}]	μ' [m^{-1}]	R^2 fit	ϵ_{SE}	T [m^{-1}]	μ' [m^{-1}]	γ	T/γ [m^{-1}]	R^2 fit	ϵ_{SE}	S	S_N	S_S
86.7	444	−72509	0.909	0.002	11904	−73597	15.22	782.0	0.996	0.008	4197	299	3.10
81.7	462	−72649	0.887	0.002	11952	−73856	14.35	833.2	0.996	0.008	4194	317	3.11
75.5	477	−72866	0.862	0.002	12016	−74330	13.26	906.4	0.993	0.009	4177	342	3.13
67.2	462	−72616	0.885	0.002	10875	−74053	11.80	921.6	0.995	0.009	4160	383	3.11
62.3	463	−72651	0.881	0.002	10574	−74234	10.94	966.7	0.992	0.010	4144	412	3.12
53.7	466	−72654	0.876	0.002	9981	−74469	9.41	1060.5	0.992	0.011	4118	475	3.11
47.0	461	−72693	0.882	0.002	9521	−74836	8.25	1153.5	0.992	0.012	4109	541	3.17
39.1	445	−72563	0.905	0.002	8607	−74955	6.87	1253.7	0.988	0.013	4079	646	3.18
33.5	422	−72353	0.931	0.002	7632	−74739	5.88	1297.5	0.983	0.014	4062	752	3.20
26.6	430	−72338	0.916	0.002	7035	−75017	4.67	1506.2	0.987	0.016	4050	943	3.19
18.9	452	−72652	0.888	0.002	7117	−76862	3.32	2144.7	0.984	0.023	3992	1308	3.25
13.6	483	−73214	0.836	0.002	7858	−80232	2.39	3290.8	0.989	0.036	3932	1802	3.33
11.0	483	−73292	0.835	0.003	7834	−81686	1.92	4070.7	0.990	0.046	3895	2210	3.35
8.0	493	−73657	0.811	0.005	8337	−85366	1.40	5950.1	0.991	0.069	3839	2996	3.41

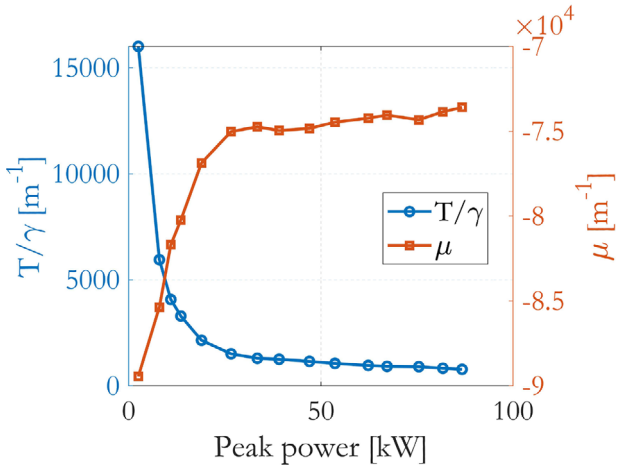

Figure 2. Temperature T/γ and chemical potential μ' (m^{-1}) versus the input peak power, in the experiment of Figure 1.

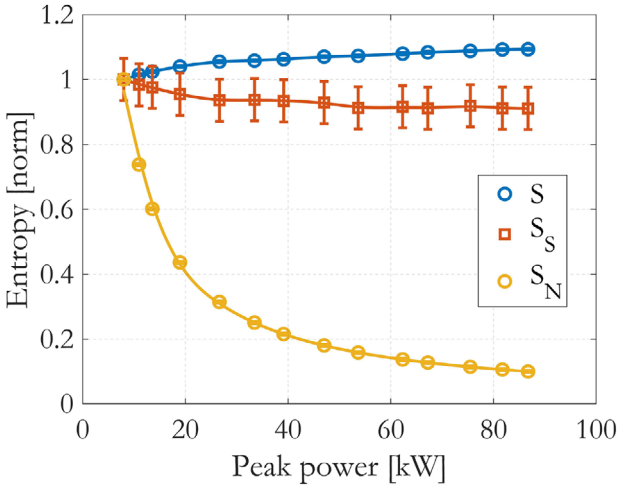

Figure 3. S, S_N and S_S, normalized to the values at the lowest power, versus the input peak power in the experiment of Figure 1.

provides the thermodynamic parameters obtained from the RJ and wBE fits. The R-square values of the wBE fit are always above 0.98, with a maximum of 0.996 at thermalization power; the R-square from the RJ range between 0.81 and 0.91 and is greater than 0.90 at 26.6 kW, which indicates that the RJ fit is accurate only in the thermalization regime. The error on state equation ϵ_{SE} ranges between 0.210 and 0.008 from the lower to higher power, and is less than 0.05 at 10.9 kW, denoting the validity of the thermodynamic approach from this power level.

The obtained larger accuracy of the wBE in terms of R-square, which allows the study of lower power regimes and higher-order modes, is related to a smaller number of approximations made in deriving Equation (6) respect to Equation (7). Conversely, the RJ provided good performance in terms of error on the state equation ϵ_{SE}; this was calculated using the second term of Equations (7) and (11).

When comparing the results obtained using the wBE or the RJ, it is clear from Equation (7) that the temperature values at different powers are to be confronted using the temperature per unit power T/γ for the wBE or $T' = 2T/\gamma$ for the RJ. Hence, starting from the wBE fits, we obtain the curves of **Figure 2** for T/γ and μ' (m^{-1}). As it was expected, the chemical potential reaches a constant value close to $-\epsilon_1 = -70672$ m^{-1} when thermalization is reached at approximately 27 kW; correspondingly, T/γ reduces to a minimum of less than 1500 m^{-1}, ten times smaller than at low power.

The values of the Boltzmann entropy S, entropy per unit particle S_N and Shannon entropy S_S, as defined in Experimental Section, are reported in **Figure 3** versus P; entropies are normalized to the values at the minimum power, and errors are reported to demonstrate the effective trends.

The error on S is calculated as $\Delta S = 2\sigma_B$, with $\sigma_B^2 = \sum_j g_j^2 \sigma_{nj}^2 / n_j^2$; $\sigma_{nj} = \Delta n_j/2$ is the standard deviation for the measurement of n_j or, equivalently, of $|f_j|^2$; in Figure 3, it was assumed $\Delta n_j/n_j = 0.1$, and statistical modal power equipartition was assumed for each group. In a similar fashion, the error on S_N is $\Delta S_N = 2\sigma_N$, with $\sigma_N^2 = \sum_j (g_j - 1)^2 \sigma_{nj}^2 / n_j^2$.

The error on S_S is calculated as $\Delta S_S = (S_S - 1)\Delta(|f_j|^2)/|f_j|^2$, coming directly from Equation (21); it was assumed $\Delta(|f_j|^2)/|f_j|^2 = 0.1$.

In Figure 3, the error on S and S_N are much smaller than for S_S, because of the n_j factor at the denominator. Despite the large error on S_S, it is confirmed its reduction as the thermalization regime is achieved. S, on the contrary, increases with power and reaches a maximum at thermalization. As expected, S_N tends to zero in the thermalization regime, despite the increase of the entropy S (see Section Experimental Section).

4. Multimode Solitons Experiment

The second set of results comes from the re-processing of previously reported experiments in the anomalous dispersion

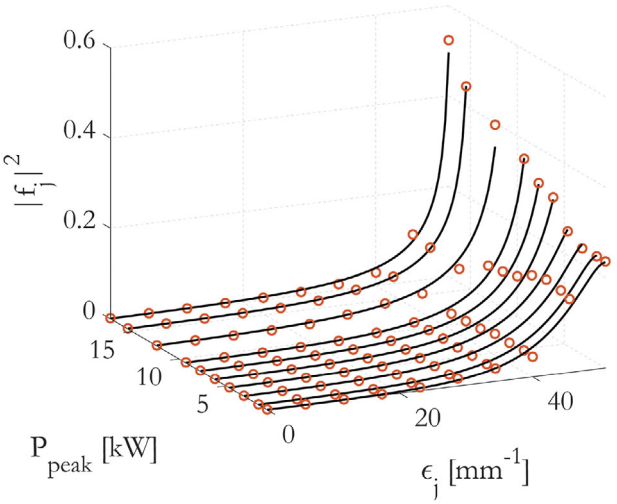

Figure 4. Output mean modal power fraction $|f_j|^2$ versus modal group eigenvalues and input peak power. 250-fs pulses were propagated over 830 m of GRIN at $\lambda = 1400$ nm. Post-processing from experimental data in Figure 2 of ref. [28]

Table 2. Thermodynamic parameters for the experiment of Figure 4.

	RJ				wBE					Entropy			
P [kW]	T' [m^{-1}]	μ' [m^{-1}]	R^2 fit	ϵ_{SE}	T [m^{-1}]	μ' [m^{-1}]	γ	T/γ [m^{-1}]	R^2 fit	ϵ_{SE}	S	S_N	S_S
17.31	388.8	−51775	0.979	0.001	10593	−52004	20.10	527	0.999	0.003	1851	92.1	2.18
15.46	418.2	−51934	0.976	0.001	10571	−52240	18.00	587	0.999	0.004	1845	102.5	2.35
12.36	525.9	−52501	0.918	0.001	11240	−53041	14.40	781	0.983	0.005	1823	126.6	2.53
9.27	511.2	−52408	0.929	0.001	9530	−53174	10.81	882	0.990	0.006	1798	166.3	2.51
7.73	538.2	−52660	0.910	0.002	9274	−53749	9.02	1029	0.988	0.007	1790	198.5	2.63
6.18	559.1	−52808	0.891	0.002	8790	−54281	7.22	1217	0.985	0.008	1762	244.0	2.64
4.64	626.3	−53414	0.809	0.002	8980	−55873	5.38	1668	0.968	0.012	1732	321.7	2.68
3.09	647.5	−53652	0.770	0.002	8337	−57361	3.59	2323	0.957	0.017	1690	470.8	2.69
1.55	655.3	−53736	0.756	0.002	7381	−59891	1.79	4113	0.959	0.031	1620	902.6	2.69
0.62	651.0	−53756	0.758	0.002	6701	−64003	0.72	9335	0.961	0.075	1533	2135.9	2.72

region.[28] Figure 2 of ref. [28] shows the propagation of 250-fs pulses into 830 m of GRIN OM4 fiber, at $\lambda = 1400$ nm, in the anomalous dispersion region of the fiber. Pulses at low power are separated by the modal dispersion, after having interacted by RMC and IM-FWM; at high power, condensation of the pulse train into solitons is achieved.

The formation of trains of quasi-solitons and solitons prevents the pulses from broadening with distance, conserving the validity of the thermodynamic approach, as it is certified by the low values of ϵ_{SE}. The mean modal power fraction was extracted using a 3D modal decomposition method, consisting of sampling the peak powers of the train of pulses, after measurement with a fast photodiode. The near-field is then reconstructed and compared with the one measured by an infrared camera.[25]

The measured mean modal power fraction, for input peak power ranging between 0.62 and 17.3 kW and for $Q = 10$ modal groups, is reported in **Figure 4**. Also, in this case, black curves are the wBE fits, showing good accuracy at all powers; for comparison, the RJ fits are reported in Figure S3 (Supporting Information).

Table 2 reports the corresponding thermodynamic parameters. The RJ fit fails to follow the HOM in the experimental data, particularly below 7.7 kW with R-square decreasing to below 0.9; regarding the wBE, the R-square ranges between 0.957 and 0.999 from lower to higher power.

The error on the state equation ϵ_{SE} ranges between 0.075 and 0.003 for the wBE, and is lower than 0.05 at $P \geq 1.55$ kW. The RJ shows good performance on ϵ_{SE}, which is limited to 0.002.

Figure 4 shows the approach to a condensed state, characterized by the content of the fundamental mode $|f_1|^2$ which increases from 0.23 to 0.53. Correspondingly, in **Figure 5** the chemical potential μ' obtained from the wBE approaches to $-\epsilon_1 = -50994$ m^{-1}, and T/γ to less than 890 m^{-1} for power larger than 10 kW, ten times smaller than at low power.

The parameter S_N and the entropy S_S in **Figure 6** experience a drop at high power, when approaching soliton condensation. The entropy S, on the contrary, increases with power and converges to a maximum. Also in this case, like in the self-cleaning experi-

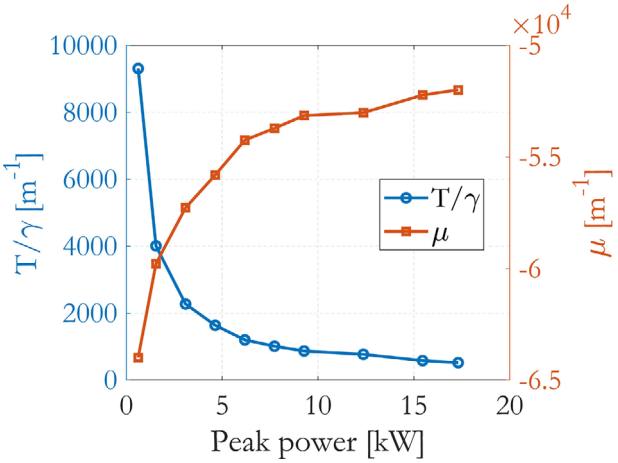

Figure 5. Temperature T/γ and chemical potential μ (m^{-1}) versus the input peak power, in the experiment of Figure 4.

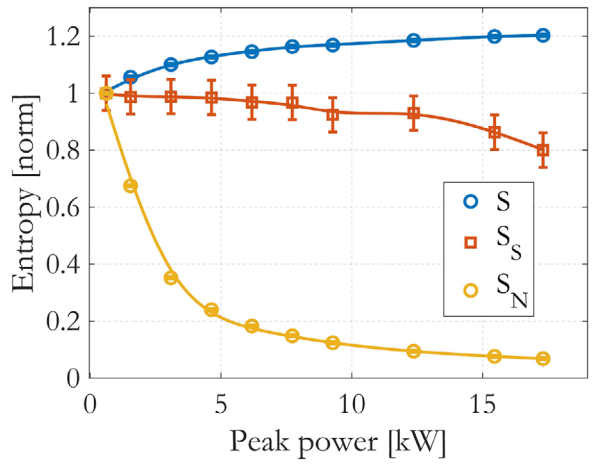

Figure 6. S, S_N and S_S, normalized to the values at the lowest power, versus the input peak power in the experiment of Figure 4.

ment, S_N and S_S reach for a minimum of information when condensation takes place.

5. Discussion and Conclusion

A new thermodynamic theory of multimode systems has been expanded respect to ref. [28], introducing new formulae for the optical entropy and the fundamental thermodynamic equation. The wBE law, Equation (1), has demonstrated good accuracy in reproducing the mean modal power distribution not only in the nonlinear thermalization regime, where IM-FWM produces intermodal mixing, but also at lower power when RMC dominates.

Experimental data from[26] and[28] have been post-processed in terms of the new theory, finding interesting analogies between the self-cleaning process in the normal chromatic dispersion region of a GRIN fiber and the soliton condensation regime in the anomalous dispersion region.

In the self-cleaning experiment, IM-FWM produced a power transfer to the lower-order groups for increasing pulse peak power; the population of the fundamental mode converged to more than 22% for $P > 19$ kW, starting from 10% at low power. The temperature per unit power T/γ, calculated using the wBE, dropped by a factor 520% for power values increasing from 11 to 86.7 kW (values where the error $\epsilon_{SE} < 0.05$); correspondingly, the chemical potential μ' approached the eigenvalue of the fundamental mode $-\epsilon_1 = -70670$ (1/m), following an abrupt change denoting a phase transition. These are clear indications of a reached thermalization state, confirmed by an increase of the Boltzmann entropy S by a factor 16%. The information entropy S_S and the entropy per unit particle S_N, on the contrary, decreased by a factor 10% and 90%, respectively.

It was demonstrated in the Experimental Section that a decrease of S_N following an increase of T, γ and S is possible under the conditions imposed by Equations (17) and (18); in the experiment, those conditions were satisfied by modes belonging to groups with $j \geq 4$, which have a larger weight for the entropy changes. The Shannon entropy S_S, on the other hand, is related to the modal occupation instead of the number of microstates; as the particles condensate to the fundamental mode, we expect to find a minimum of information in terms of modal distribution.

In the soliton condensation experiment, a complex interplay of modal dispersion, RMC and IM-FWM results in the generation of a single pulse or a train of pulses propagating as quasi-solitons or solitons, depending on the input power and coupling conditions.[28] In the absence of RMC, pulses carrying the individual modal groups would be lacking the modes from other groups or the fundamental mode. RMC generates a background noise composed of all modes which contribute to populate the propagating pulses. IM-FWM therefore transfers power to the lower order modes present in all pulses, generating a single soliton or a train of condensed solitons. In this context, it was observed a modal power re-distribution for increasing P, with the power fraction of the fundamental mode passing from 23% to 52% from the lower to the higher power. T/γ decreased by a factor 780% when passing from 1.55 to 17.3 kW (corresponding to $\epsilon_{SE} < 0.05$). In the same power range, the μ' increased approaching to $-\epsilon_1 = -51000$ (1/m); also in this case an abrupt change was observed, indicating a phase transition. The entropy S increased by a factor 14%, S_S and S_N decreased of 19% and 90%, respectively.

The operative difference between the two regimes is principally the fiber length. In self-cleaning experiments, the most detrimental effect of the validity of the thermodynamic approach is chromatic dispersion, which can be considered as a dissipative effect itself. In nonlinear thermodynamics, the number of particles N is proportional to the pulse peak power P, because the modal power redistribution is caused by the IM-FWM nonlinear effect. As a consequence of chromatic dispersion, pulse broadens by a factor $\sqrt{2}$ after a dispersion length $L_D = T_0^2/\beta_2$, being T_0 the pulse width and β_2 (s^2/m) the fiber dispersion; the peak power P and peak number of particles N decrease accordingly, producing an error ϵ_{SE} which may go well above 5%. fiber length is therefore limited to few meters and, in some cases, less than 1 m. For high pulse peak power, self-phase modulation (SPM) induces nonlinear phase chirp and spectral broadening; however, pulse shape is not affected by the interplay of SPM and chromatic dispersion, because of the reduced fiber length.

In soliton condensation experiments, RMC is a necessary step to produce a single condensed pulse or a train of pulses. Pulse broadening is compensated by self-phase modulation (SPM), hence, the chromatic dispersion does not act as a dissipative effect. Long distances (hundred of meters) are necessary to observe a power transfer to the fundamental mode because of the interplay between modal dispersion, RMC and IM-FWM. RMC generates a limited change to the internal energy because of particle transfer to other groups; if, for example, a complete transfer of power is produced by RMC from the modal group $j = 10$ to $j = 1$ the energy change is $(\beta_{j=10} - \beta_{j=1})/\beta_{j=10} \leq 0.008$. For fully formed solitons, at power higher that those considered here, inter-modal stimulated Raman scattering (IM-SRS)[31,32] is responsible for wavelength red-shift of the formed solitons; in this case, a wavelength shift $\lambda_2 - \lambda_1 = 80$ nm produces a change to the internal energy of $[\beta(\lambda_2) - \beta(\lambda_1)]/\beta(\lambda_1) \leq 0.05$. Hence, a limited Raman nonlinearity as well as RMC can be compatible with the thermodynamic approach, and the error ϵ_{SE} must be used as an overall check for the thermodynamic validity of the experiment.

The surprising similarities between the results of the two experiments, which involve all the thermodynamic parameters, indicate a common basis for condensation processes in the normal and anomalous chromatic dispersion regimes. Beam self-cleaning and soliton condensation are both caused by IM-FWM as the primary process, and both are observed at P ranging between 10 and 30 kW. Thermodynamics based on wBE has proven to be a powerful tool for the analysis of processes which are different from an operational point of view, but similar in thermodynamic terms.

Higher power regimes respect to those observed in the experiments cause a strong Raman self-frequency shift (RFFS) and fission in the soliton regime. In the normal dispersion regime, pulses experience nonlinear losses for peak power above 600 kW[33] causing a reduction of the internal energy. When Raman shift in the soliton regime, or multi-photon absorption in the normal dispersion regime, cause an excessive variation of internal energy U, the thermodynamic approach is invalidated.

6. Experimental Section

Weighted Bose–Einstein and Raileigh–Jeans Laws: In the main text, it was considered an optical multimode system including Q groups of degenerate modes, distributed over $g_j/2$ modes and 2 polarizations, with $j = 1, 2, .., Q$; hence, g_j is the degeneracy over two polarizations. In the special case of a GRIN fiber, it is $g_j = 2, 4, 6, .., 2Q$; the number of modes and polarizations is $2M = Q(Q+1)$.

The nearly degenerate modes of a group have substantially equal propagation constant[29]

$\beta_j = n_{co}k_0\sqrt{1-2\Delta(j/Q)}$ (m^{-1}), with n_{co} the core index and $\Delta = (n_{co}^2 - n_{cl}^2)/2n_{co}^2$ the relative core-cladding index difference.

Suppose that n_j is the bosonic population into modal group j, distributed over g_j nearly-degenerate modes and polarizations. $\epsilon_j = \beta_j - \beta_{j=Q}$ are the differential modal eigenvalues. The total number of particles in the system $N = \sum_{j=1}^{Q} n_j$. Power can be written as $P = \sum_{j=1}^{Q} n_j P_0/n_0$ (in units of W); the system's internal energy is $U = -\sum_{j=1}^{Q} \beta_j n_j P_0/n_0$ (in units of W/m). $\gamma = N/n_0 = P/P_0$ is the total fractional power, with n_0 a reference number of particles and P_0 the corresponding input peak power.

Physical processes such as IM-FWM and RMC are capable of mixing power among the modes and modal groups with negligible effect on the total power and internal energy, the latter process being effective over long distances. The multiplicity of the system, defined as the number of possible microstates populated by the particles, is given by

$$W = \prod_{j=1}^{Q} \frac{(n_j + g_j - 1)!}{n_j!(g_j-1)!} \tag{3}$$

The Boltzmann entropy of the system $S = \ln(W)$ is related to the number of microstates; it reads[18]

$$S = \sum_{j=1}^{Q} (n_j + g_j - 1)\Big[\ln(n_j + g_j - 1) - 1\Big] - (g_j - 1)\Big[\ln(g_j - 1) - 1\Big] - n_j\Big[\ln(n_j) - 1\Big] \tag{4}$$

The quantity $S_N = S/\gamma = n_0 \ln(W)/N$ has the meaning of an entropy per unit power; although it cannot be considered as an entropy itself (for example, it is not additive), an extremum of S_N can be sought while assuming constant the system's normalized internal energy $U_N = U/P = -\sum_j \beta_j n_j/N$ (1/m) and the power $P_N = P/P = \sum_j n_j/N = 1$ (both are normalized to the power $P = \gamma P_0 = NP_0/n_0$)

$$\frac{\partial}{\partial n_l}\left[\ln(W)/N + \sum_{j=1}^{Q}\left(an_j/N + b\beta_j n_j/N\right)\right] = 0 \tag{5}$$

Equation (5) is multiplied by N and solved using two possible sets of Lagrange multipliers (a, b) or (a', b').[28] A first solution, related to the choice (a, b), is the weighted Bose–Einstein law (wBE)

$$|f_j|^2 = \frac{2(g_j-1)}{g_j\gamma}\frac{1}{\exp\left(-\frac{\mu'+\epsilon_j}{T}\right) - 1} \tag{6}$$

in Equation (6), $|f_j|^2 = 2n_j/(\gamma n_0 g_j)$ is the mean modal power fraction in modal group j, over two polarizations. $\mu' = \mu + \beta_{j=Q}$, with μ (1/m) a chemical potential and T (1/m) an optical temperature. μ' and T are two degrees of freedom for fitting Equation (6) to the experimental data. The γ parameter is free at only one intermediate power; for other powers, it must scale proportionally to P or N; the second constraint is the respect of the conservation law $\sum_{j=1}^{Q}(g_j/2)|f_j|^2 = 1$.

Hence, the wBE distribution is valid in experiments where $U_N = const$, or equivalently, where γ and U scale proportionally or they are constant.

A second solution, related to the choice (a', b'), is obtained under the assumption $|\mu' + \epsilon_i| << |Tn_0|$, which leads to the Rayleigh–Jeans (RJ) distribution:

$$|f_j|^2 = -\frac{2(g_j-1)}{g_j\gamma}\frac{T}{\mu' + \epsilon_j} \simeq -\frac{T'}{\mu' + \epsilon_j} \tag{7}$$

with $T' = 2T/\gamma$ (1/m). In Equation (7), the power factor γ was included into the temperature T'; hence, T' has meaning similar to the parameter T/γ of the wBE, when comparing the results obtained from Equations (6) and (7).

The two sets of Lagrange multipliers used to obtain Equations (6) and (7) bring to the same values of internal energy and power, namely[28]

$$\sum_{j=1}^{Q}(a' + b'\beta_j)n_j = \sum_{j=1}^{Q} an_j + b\beta_j n_j = Q - 2M = \frac{\mu N}{Tn_0} + \frac{1}{Tn_0}\left(-\frac{UN}{P}\right) \tag{8}$$

which provides a common state equation (SE)

$$U - \mu P = (2M - Q)P_0 T \tag{9}$$

The SE can be rewritten in terms of $U_N = U/P$, γ and fitting parameters μ' and T

$$SE = -U_N + \mu + V\frac{T}{\gamma} = \sum_{j=1}^{Q}\beta_j\frac{g_j}{2}|f_j|^2 + \mu' - \beta_{j=Q} + V\frac{T}{\gamma} = 0 \tag{10}$$

where $V = (2M - Q)$ was introduced as the system volume. The experimental error on the SE can be calculated as

$$\epsilon_{SE} = \frac{SE}{\sum_{j=1}^{Q}\beta_j\frac{g_j}{2}|f_j|^2 - \left(\mu' - \beta_{j=Q} + V\frac{T}{\gamma}\right)} \tag{11}$$

The error ϵ_{SE} can be used to certify the validity of the thermodynamic approach. Experimental data show that an error of less than 1% is obtained when approaching to the system thermalization or condensation.

The thermodynamic approach is not limited to GRIN fibers but applies to multimode optical system such as waveguide arrays and lattices.[18] In a recent preprint paper,[34] wBE thermodynamics was experimentally investigated in linear GRIN fibers, where RMC is the only responsible for power exchange among modes and modal groups; experiments were repeated in single-photon pulse quantum regime, demonstrating the ergodicity of the RMC process.

Optical Entropy: The Boltzmann entropy (Equation (4)) can be approximated for $n_j >> g_j$ to

$$S = \sum_{j=1}^{Q}(g_j - 1)\ln(n_j) \tag{12}$$

In the literature,[18,35] Equation (12) is reduced, in the case of unitary degeneracy, to $S = \sum_{i=1}^{M}\ln(n_i) + M$.

Using Equations (6) and (9) for the wBE and the SE, It is obtained.

$$S = -\sum_{j=1}^{Q}(g_j - 1)\ln\left[\frac{\exp\left(-\frac{\beta_j}{T} - \frac{U_N}{T} + \frac{V}{\gamma}\right) - 1}{n_0(g_j - 1)}\right] \tag{13}$$

By considering the normalized internal energy U_N, number of particles γ and volume V as dependent on T, derivatives are calculated as

$(\partial S/\partial X)_Y = \partial S/\partial X + (\partial S/\partial T)(\partial T/\partial X)$, with $X, Y = U_N, \gamma, V$ or T, obtaining the fundamental equation

$$dS = \sum_{j=1}^{Q} q_j \left[\frac{\gamma}{T} dU_N - \frac{\mu}{T} d\gamma - dV - \gamma \left(\frac{\beta_j + U_N}{T^2} \right) \left(\frac{\partial T}{\partial U_N} dU_N + \frac{\partial T}{\partial \gamma} d\gamma + \frac{\partial T}{\partial V} dV + dT \right) \right] \tag{14}$$

with weight factor

$$q_j = \frac{g_j}{2} |f_j|^2 \exp\left(-\frac{\mu' + \epsilon_j}{T} \right) \tag{15}$$

In Equation (15), the modal group fractions multiply the weight $\exp[-(\mu' + \epsilon_j)/T]$, which in multimode fibers is larger than 500 for modal group $j = 14$ and approaches to less than 10 for the fundamental mode; hence, populated HOMs mostly contribute to the entropy changes. It is therefore important to use fitting laws which accurately describe also the HOM content, like the wBE.

In experiments involving proportional changes of U and γ, like those considered in this work, the normalized energy $U_N = U/\gamma P_0$ is constant (the normalized number of particles is always unity). In this case, reference must be made to the quantity $S_N = S/\gamma$ which, although non representing an entropy, is extremized by Equation (5) under the constraint $U_N = const$ and brings in any case to the wBE and RJ. Therefore, for the experiments considered in this work, it is meaningful to calculate this quantity too. After derivatives with respect to U_N, γ, T and $V = 2M - Q$ it was obtained

$$dS_N = \sum_{j=1}^{Q} q_j \left[\frac{dU_N}{T} + \frac{U_N - \mu}{\gamma T} d\gamma - \frac{dV}{\gamma} - \frac{\beta_j + U_N}{T^2} \left(\frac{\partial T}{\partial U_N} dU_N + \frac{\partial T}{\partial \gamma} d\gamma + \frac{\partial T}{\partial V} dV + dT \right) \right] \tag{16}$$

In Equations (14) and (16) the volume can be considered as a constant ($dV = 0$); in fact, the number of supported modes depend on the multimode architecture and not on the input power or modal distribution. Alternatively, the number of modes M and groups Q is dependent on the experimental accuracy for the modal fraction of the HOMs; it is reasonable to limit the number of groups Q to those measurable within a given accuracy.

In those experiments where the non-normalized energy and power are constant ($dU = d\gamma = 0$) it was found from Equation (14) that $dS > 0$ for $-\gamma(\beta_j + U_N)dT/T^2 > 0$. Hence, by using Equation (9), an increase of the entropy is obtained following an increase of the temperature ($dT > 0$) for

$$\beta_j < -U_N \tag{17}$$

Since populated HOMs have much larger weight in Equation (14), it is important that Equation (17) is satisfied for the populated HOMs and not necessarily for the lower-order groups. The weights q_j imply the need to use thermodynamic laws capable of reproducing the distribution of the HOMs, such as the wBE.

In the experiments considered in this work, it is $dU_N = dV = 0$; from Equation (14) an increase of entropy ($dS > 0$) was observed for

$$-\frac{\mu}{T} d\gamma > \gamma \frac{\beta_j + U_N}{T^2} \left(\frac{\partial T}{\partial \gamma} d\gamma + dT \right) \tag{18}$$

the first term in Equation (18) is always positive for $d\gamma > 0$; if $dT > 0$ was also assumed, Equation (18) is valid whenever Equation (17) is satisfied at least for the HOMs with larger weight. For example, in the self-cleaning experiments analyzed in this work (Figure 1), Equation (17) is satisfied for group orders with $j \geq 4$.

The aim was to demonstrate that it is possible to obtain a decrease of the entropy per unit particle $dS_N < 0$ after an increase of the entropy ($dS > 0$) and of the temperature with the input power ($dT/d\gamma > 0$). From Equation (16), assuming $dU_N = dV = 0$ and using again Equation (9), a decrease of S_N is possible for

$$\frac{dT}{d\gamma} > \frac{T^2 V}{\gamma^2 (\beta_j + U_N)} \tag{19}$$

if Equations (17) is satisfied, it is $dS > 0$ from Equation (18) and the second term in Equation (19) is negative; hence, the equation is always true for $dT/d\gamma > 0$.

Interest was also directed toward considering the information or Shannon entropy S_S, related to the classical concept of modal occupation instead of microstates distribution. In this case, reference must be made to the M modes with population $m_i = N|f_i|^2$, $i = 1, 2, .., M$; the modes are not distinguished by polarization, and it still results $2M = Q(Q + 1)$. The system multiplicity is reformulated in this case as ref. [36]

$$W_S = \frac{N!}{\prod_{i=1}^{M} m_i!} \tag{20}$$

the Shannon entropy is calculated per unit particle as

$$S_S = \frac{\ln(W_S)}{N} = \frac{1}{N} \left[\ln(N!) - \sum_{i=1}^{M} \ln(m_i!) \right] \simeq \frac{1}{N} \left[N \ln(N) - \sum_{i=1}^{M} N|f_i|^2 \ln(N|f_i|^2) \right] == - \sum_{i=1}^{M} |f_i|^2 \ln(|f_i|^2) \tag{21}$$

in Equation (21), it was applied the Stirling's approximation, valid for $m_i >> 1$, and also $\sum_{i=1}^{M} |f_i|^2 = 1$. For systems with degeneracy and assuming statistical modal power equipartition into the groups, it is $|f_j| = |f_i|$ for groups with g_j modes and polarizations, and mode index i corresponding to group index j. Namely, for a GRIN fiber, it is $g_j = 2$ and $i = 1$ for $j = 1$, $g_j = 4$ and $i = \{1, 2\}$ for $j = 2$, up to $g_j = 2Q$ and $i = \{j(j + 1)/2) - j + 1, .., j(j + 1)/2\}$ for $j = Q$. The Shannon entropy can be rewritten in this case as

$$S_S = - \sum_{j=1}^{Q} \frac{g_j}{2} |f_j|^2 \ln(|f_j|^2) \tag{22}$$

As a final remark, the notation of Equation (12) must be harmonized with that used in the literature.[18,35] Assuming for simplicity unitary degeneracy of the modal groups, with two propagating polarizations per mode, it is $g_j \equiv 2$ and $Q = M$. The Boltzmann entropy is expressed as

$$S = \sum_{i=1}^{M} \ln(n_i) = \sum_{i=1}^{M} \ln\left(\frac{N}{P} |c_i|^2 \right) = M \ln\left(\frac{N}{P} \right) + \sum_{i=1}^{M} \ln(|c_i|^2) \tag{23}$$

The first term on the right-hand side of Equation (23) is a constant; the second term is expressed in Watt and depends on the input power according to $|c_i|^2 = P|f_i|^2$. Hence, the second term is a non-normalized Boltzmann entropy, which is a particular case of Equation (12) and cannot be reduced to the Shannon entropy of Equation (21).

Supporting Information

Supporting Information is available from the Wiley Online Library or from the author.

Acknowledgements

The author wishes to thank F. Wise, H. Pourbeyram and F. Wu for fruitful discussions and for making freely available the self-cleaning data processed in this work. Project ECS 0000024 Rome Technopole, - CUP B83C22002820006, Funded by the European Union - NextGenerationEU.

Conflict of Interest

The authors declare no conflict of interest.

Data Availability Statement

The data that support the findings of this study are available from the corresponding author upon reasonable request.

Keywords

disorder, multimode fibers, nonlinear optics, self-cleaning, solitons

Received: May 17, 2024
Revised: December 8, 2024
Published online:

[1] D. Gloge, E. A. J. Marcatili, *Bell Syst. Tech. J.* **1973**, *52*, 1563.
[2] A. Hasegawa, *Opt. Lett.* **1980**, *5*, 416.
[3] D. J. Richardson, J. M. Fini, L. E. Nelson, *Nat. Photonics* **2013**, *7*, 354.
[4] P. J. Winzer, D. T. Neilson, A. R. Chraplyvy, *Opt. Express* **2018**, *26*, 24190.
[5] R.-J. Essiambre, G. Kramer, P. J. Winzer, G. J. Foschini, B. Goebel, *J. Lightwave Technol.* **2010**, *28*, 662.
[6] L. G. Wright, D. N. Christodoulides, F. W. Wise, *Science* **2017**, *358*, 94.
[7] D. Leykam, S. Flach, *APL Photonics* **2018**, *3*, 070901.
[8] N. O. Moussa, T. Mansuryan, C.-H. Hage, M. Fabert, K. Krupa, A. Tonello, M. Ferraro, L. Leggio, M. Zitelli, F. Mangini, et al., *Sci. Rep.* **2021**, *11*, 1.
[9] V. E. Zakharov, V. S. L'vov, G. Falkovich, *Statistical Description of Weak Wave Turbulence*, Springer Berlin Heidelberg, Berlin, Heidelberg **1992**, pp. 63–82.
[10] A. Picozzi, J. Garnier, T. Hansson, P. Suret, S. Randoux, G. Millot, D. Christodoulides, *Phys. Rep.* **2014**, *542*, 11.
[11] T. Markvart, *J. Opt. A: Pure Appl. Opt.* **2007**, *10*, 015008.
[12] C. Conti, M. Leonetti, A. Fratalocchi, L. Angelani, G. Ruocco, *Phys. Rev. Lett.* **2008**, *101*, 143901.
[13] L. G. Wright, D. N. Christodoulides, F. W. Wise, *Nat. Photonics* **2015**, *9*, 306.
[14] W. H. Renninger, F. W. Wise, *Nat. Commun.* **2013**, *4*, 1.
[15] K. Krupa, A. Tonello, B. M. Shalaby, M. Fabert, A. Barthélémy, G. Millot, S. Wabnitz, V. Couderc, *Nat. Photonics* **2017**, *11*, 237.
[16] K. Baudin, A. Fusaro, K. Krupa, J. Garnier, S. Rica, G. Millot, A. Picozzi, *Phys. Rev. Lett.* **2020**, *125*, 244101.
[17] K. Baudin, J. Garnier, A. Fusaro, C. Michel, K. Krupa, G. Millot, A. Picozzi, *Opt. Commun.* **2023**, *545*, 129716.
[18] F. O. Wu, A. U. Hassan, D. N. Christodoulides, *Nat. Photonics* **2019**, *13*, 776.
[19] K. G. Makris, F. O. Wu, P. S. Jung, D. N. Christodoulides, *Opt. Lett.* **2020**, *45*, 1651.
[20] D. Gloge, *Bell Syst. Tech. J.* **1972**, *51*, 1767.
[21] S. Savović, A. R. Simović, B. Drljaća, A. Djordjevich, G. Stepniak, C.-A. Bunge, J. S. Bajić, *J. Lightwave Technol.* **2019**, *37*, 4985.
[22] N. Berti, K. Baudin, A. Fusaro, G. Millot, A. Picozzi, J. Garnier, *Phys. Rev. Lett.* **2022**, *129*, 063901.
[23] A. Fusaro, J. Garnier, K. Krupa, G. Millot, A. Picozzi, *Phys. Rev. Lett.* **2019**, *122*, 123902.
[24] Q. Zhong, F. O. Wu, A. U. Hassan, R. El-Ganainy, D. N. Christodoulides, *Nat. Commun.* **2023**, *14*, 370.
[25] M. Zitelli, V. Couderc, M. Ferraro, F. Mangini, P. Parra-Rivas, Y. Sun, S. Wabnitz, *Photon. Res.* **2023**, *11*, 750.
[26] H. Pourbeyram, P. Sidorenko, F. O. Wu, N. Bender, L. Wright, D. N. Christodoulides, F. Wise, *Nat. Phys.* **2022**, *18*, 685.
[27] K. Krupa, A. Tonello, B. M. Shalaby, M. Fabert, A. Barthélémy, G. Millot, S. Wabnitz, V. Couderc, *Nat. Photonics* **2017**, *11*, 237.
[28] M. Zitelli, F. Mangini, S. Wabnitz, *Nat. Commun.* **2024**, *15*, 1149.
[29] R. Olshansky, *Appl. Opt.* **1975**, *14*, 935.
[30] L. G. Wright, F. O. Wu, D. N. Christodoulides, F. W. Wise, *Nat. Phys.* **2022**, *18*, 1018.
[31] J. P. Gordon, *Opt. Lett.* **1986**, *11*, 662.
[32] M. Zitelli, M. Ferraro, F. Mangini, S. Wabnitz, *J. Lightwave Technol.* **2022**, *40*, 7914.
[33] M. Ferraro, F. Mangini, M. Zitelli, A. Tonello, A. De Luca, V. Couderc, S. Wabnitz, *Photonics Res.* **2021**, *9*, 2443.
[34] M. Zitelli, *arXiv:2409.18795* **2024**.
[35] G. Yang, D. Bongiovanni, D. Song, R. Morandotti, Z. Chen, N. K. Efremidis, *APL Photonics* **2024**, *9*, 066115.
[36] E. T. Jaynes, *Probability Theory: The Logic of Science*, Cambridge University Press, Cambridge **2003**.